Modelling mass and heat transfers of permeate pap membrane distillation using hollow fibre membrane

Modelling mass and heat transfers of Permeate Gap Membrane Distillation using hollow fibre membrane

Li Gao[a,b], Jianhua Zhang[a], Stephen Gray[a], Jun-De Li[a*]

[a] Institute of Sustainability and Innovation, College of Engineering and Science, Victoria University, PO Box 14428, Melbourne, Victoria, 8001, Australia

[b] South East Water Corporation, PO Box 2268 Seaford Victoria, 3198, Australia

Abstract

In this study, a set of mathematical models was used to simulate the heat and mass transfers of hollow fibre PGMD module for desalination applications. The developed model was firstly validated, and then utilized to study the impacts of different design parameters and operating conditions on the performance of hollow fibre PGMD. The simulation results show that coolant velocity and coolant temperature have less impacts on flux compared to those in DCMD, because in DCMD, coolant directly contacts the membrane but for PGMD it does not. The model also demonstrates that the higher cooling plate thermal conductivity will lead to higher flux and energy efficiency. However, when the cooling plate thermal conductivity is higher than 5 W/m.K, the temperature difference across the cooling plate is minimum and further increase of the cooling plate thermal conductivity has negligible impacts on flux and energy efficiency. A sensitivity analysis was undertaken to analyze the combined effects of gap channel inner/outer diameters and gap channel thermal conductivity on flux. It is concluded that the changes in gap channel of hollow fibre PGMD will lead to a more complex combination, and the gap channel thermal conductivity has a more significant effect on flux compared to the hydrodynamics within the permeate and coolant channels. The effect of multi-stage processes on energy efficiency is also evaluated. The results suggest that Gain Output Ratio (GOR) increases with number of stages, and reaches 2.4 with 20 stages. Finally, the roles of different parameters in PGMD optimization are discussed. The results suggest that cooling plate thermal conductivity plays the most important role in PGMD optimization compared to coolant velocity and coolant inlet temperature.

Keywords: Hollow fibre membrane, Permeate Gap Membrane Distillation, sensitivity analysis, multi-stage process

1. Introduction

With the increasing focus on better product quality and higher energy efficiency, Membrane Distillation (MD) has been recognized as a potential alternative for desalination applications. The operation of MD is based on the different vapour pressures established across a hydrophobic membrane [1]. In MD, the feed solution is vapourized at the membrane surface of the feed side, the vapour penetrates through the hydrophobic membrane, afterwards, it is either condensed into permeate at the interface between the membrane and coolant or removed by sweeping gas. The MD working principle enables the potential use of alternative heat sources and low-grade thermal energy [2-5], which is a key advantage compared to conventional distillation and membrane filtration processes. Furthermore, its purification process involves the phase-changes (liquid-gas-liquid), enabling a high quality of the permeate [6].

Permeate Gap Membrane Distillation (PGMD) and its modified designs [7, 8] are developed based on re-arrangement of the coolant channel, exhibiting various benefits compared to other MD configurations. For PGMD configuration, an additional gap (permeate gap) is established in the middle to separate the membrane from the coolant. The gap is filled by gradually produced permeate, and the coolant channel is placed on the other side of the permeate gap. This new coolant channel arrangement enables internal heat recovery within the MD module [9]. Furthermore, because the coolant contacts gap channels rather than the membrane directly, the sensible heat loss is reduced compared to Direct Contact MD (DCMD). The mass transfer of PGMD is also enhanced compared to Air Gap MD (AGMD) because of the elimination of air gap. However, the thermal conductivity of water is considerably higher than that of air, PGMD has a less heat transfer resistance within the permeate gap compared to AGMD, which results in a higher sensible heat loss. The heat and mass flows for PGMD are shown diagrammatically in Fig. 1.

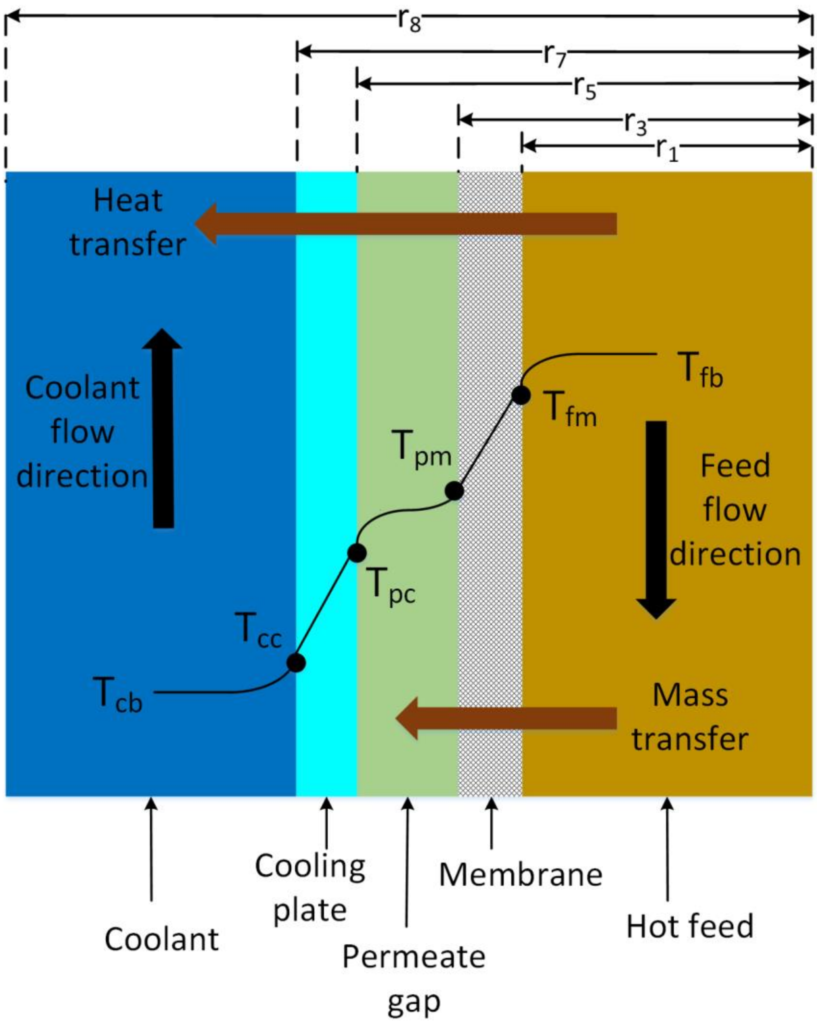

Fig. 1. Overview of heat and mass flows of PGMD

In Fig. 1, T_{fb}, T_{fm}, T_{pm}, T_{pc}, T_{cc}, and T_{cb} are the bulk feed temperature, interface temperature between feed and membrane, interface temperature between permeate and membrane, interface temperature between permeate and cooling plate, interface temperature between coolant and cooling plate, and bulk coolant temperature, respectively.

Even though PGMD concept has been investigated by different researchers [7-20], previous studies focused on spiral wound and flat sheet PGMD. The structure of the flat sheet PGMD module is generally simple and it is relatively easy to manufacture, however, it has a low packing density (specific surface area) compared to hollow fibre or spiral wound modules. Spiral wound PGMD module usually has a high energy efficiency due to the maximized internal heat recovery, but its permeation flux is very low, which is due to the low temperature difference between membrane surfaces. Gao et al. [9] compared the PGMD performance in different module designs and concluded that a more balanced result between flux and energy consumption could be achieved by hollow fibre PGMD module compared to other PGMD configurations (spiral wound or flat sheet).

A better insight into the mass and heat transfers phenomenon within the PGMD module and the impacts of different design parameters will facilitate the future scale-up of hollow fibre PGMD module. Gao et al. [20] investigated the impacts of various design parameters on flux and energy performance using different hollow fibre PGMD module designs. That study also suggested different approaches (effective membrane surface increase, multi-stage process, etc.) to further optimize hollow fibre PGMD performance.

To optimize PGMD module design more efficiently, a set of mathematical models are developed and implemented in a computer program using MATLAB to simulate the heat and mass transfer phenomena of PGMD process. To the best of authors' knowledge, this is the first study to undertake a systematic analysis of heat and mass transfers of hollow fibre PGMD module and to build the mathematical model accordingly. Due to the unique module design, the developed model takes both gap channel density and hollow fibre packing density into consideration, suggesting that hollow fibres could attach to each other and lose their full contacts with permeate when hollow fibre packing density is high. In addition, the developed model considers convection and conduction phenomenon for the heat transfer within the gap channel due to the existence of water gap rather than the air gap. This is different from AGMD, where the heat transfer within the air gap is described by sensible heat conduction and latent heat transfer. Furthermore, the developed model enables a discussion on the role of cooling plate thermal conductivity and its limitation. Based on the modelling results, the design of hollow fibre PGMD module could be further optimized.

2 PGMD process simulation

2.1 Theoretical analysis of mass and heat transfers of PGMD

The heat and mass transfers of PGMD process can be analyzed in each small segment dx along the module (see Fig. 2) based on the following 5 sub-processes. It is assumed that the feed flows counter-current to the coolant stream.

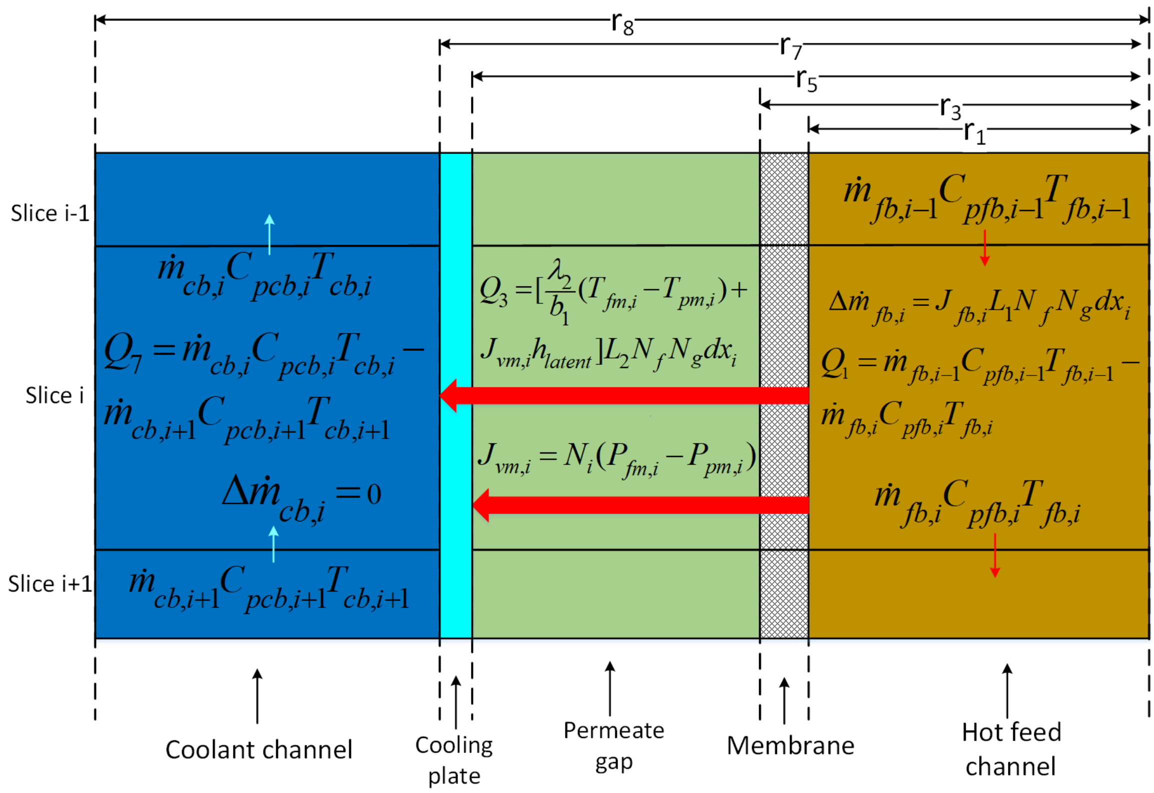

Fig. 2. Analysis of heat and mass transfers from slice *i-1* to slice *i+1* along PGMD module

2.1.1 Mass and heat transfers in hot feed channel

The mass transfer phenomenon of hot feed channel for slice i can be described by:

$$\Delta\dot{m}_{fb,i}=\dot{m}_{fb,i-1}-\dot{m}_{fb,i}=J_{fb,i}L_1N_fN_gdx_i \tag{1}$$

The heat transfer of slice i for the hot feed channel is described below:

$$Q_1=\dot{m}_{fb,i-1}C_{pfb,i-1}T_{fb,i-1}-\dot{m}_{fb,i}C_{pfb,i}T_{fb,i} \tag{2}$$

$$L_1=2\pi r_1 \tag{3}$$

Here, the subscript i represents the i^{th} slice; $\Delta\dot{m}_{fb,i}$ represents the change of mass flow rate for the feed bulk flow; $J_{fb,i}$ represents the water vapour flux of hot feed channel; $\dot{m}_{fb,i}$ and

$\dot{m}_{fb,i-1}$ indicate the bulk feed mass flow rates coming out and into the slice, respectively; Q_1 represents total heat transfer rate of hot feed channel; L_1 represents the circumference of hollow fibre membrane based on its inner diameter; $C_{pfb,i}$ and $C_{pfb,i-1}$ are the specific heat capacities of feed bulk flow coming out and into the slice, respectively; $T_{fb,i}$ and $T_{fb,i-1}$ are temperatures for feed bulk flow coming out and into the slice, respectively; N_f represents the number of hollow fibre membrane that each gap channel accommodates; N_g represents the number of gap channels; dx_i represents the length of the slice i; and r_1 is defined as the inner radius for the employed hollow fibre.

It is worthwhile mentioning that the hot feed vapourizes at the interface between the membrane and feed solution, and the feed solution flows through the membrane lumen side. Therefore, the heat transfer coefficient for the heat transfer from the feed to the membrane is that at the inner surface of the hollow fibre. Consequently, the hollow fibre inner radius r_1 is used to calculate the interface surface area for mass/heat transfers in the hot feed channel.

Based on the above information, the heat transfer from the hot bulk flow to the hollow fibre membrane surface at hot feed side can be described by:

$$Q_2 = \alpha_{f,i}(T_{fb,i} - T_{fm,i})L_1 N_f N_g dx_i \tag{4}$$

Here Q_2 represents total heat transfer; $T_{fm,i}$ represents the temperature of the interface between hollow fibre membrane and hot feed; and $\alpha_{f,i}$ represents the heat transfer coefficient at the hot feed side, which can be described by [21]:

$$\alpha_{f,i} = \frac{Nu_f \lambda_1}{d_{hf}} \tag{5}$$

Here λ_1 represents the feed brine thermal conductivity; d_{hf} is the hydraulic diameter for the feed channel, which can be determined by:

$$d_{hf} = \frac{4A_1}{L_1} = 2r_1 \tag{6}$$

Here, A_1 is the cross sectional area for the hot channel based on its inner diameter. Nu_f is the Nusselt's number of the hot feed. Previous experimental results [9] suggested that the water within the feed channel, permeate gap and coolant channel all had laminar flow regimes. Consequently, Nu_f under fully developed flow and uniform heat flux condition can be calculated by [22, 23]:

$$Nu_f = 4.36 + \frac{0.036(\mathrm{Re}\,\mathrm{Pr}\,d_{hf}/l)}{1+0.0011(\mathrm{Re}\,\mathrm{Pr}\,d_{hf}/l)^{0.8}} \tag{7}$$

Here, l represents the length of the module; Pr and Re represent Prandtl number and Reynolds number, respectively, which can be calculated by:

$$\mathrm{Pr} = \frac{C_p \mu}{\lambda} \tag{8}$$

$$\mathrm{Re} = \frac{\rho d_h v}{\mu} \tag{9}$$

Here, C_p, ρ, μ, d_h, v and λ are specific heat capacity, density, viscosity, hydraulic diameter, velocity, and thermal conductivity of water, respectively. The thermodynamic properties and viscosities are allowed to vary with temperature which changes along the module length, Re and Pr are respectively calculated for hot and coolant channels using Eqs. (8 – 9).

2.1.2 Mass and heat transfers through hollow fibre membrane

The mass transfer phenomenon for slice *i* through the hollow fibre is expressed by:

$$J_{vm,i} L_2 N_f N_g dx_i = N_i (P_{fm,i} - P_{pm,i}) L_2 N_f N_g dx_i \tag{10}$$

Here $J_{vm,i}$ represents the vapour mass flux through hollow fibre, it is slightly smaller than $J_{fb,i}$ due to difference between L_1 and L_2; N_i is the mass transfer coefficient for hollow fibre membrane; $P_{fm,i}$ and $P_{pm,i}$ are vapour pressures at the membrane interfaces corresponding to temperatures $T_{fm,i}$ and $T_{pm,i}$, respectively; and L_2 indicates the average circumference based on average radius r_2, which can be calculated by the hollow fibre inner radius (r_1) and outer radius (r_3):

$$L_2 = \frac{2\pi(r_3 - r_1)}{\ln(r_3 / r_1)} \quad (11)$$

Because the total pressure difference does not exist inside membrane pores, the effect of viscous flow is negligible for PGMD, the mass transfer phenomenon through hollow fibre membrane is determined by Knudsen-molecular diffusion transition mechanism [10]. As a result, N_i can be calculated by [21]:

$$N_i = (\frac{1-\chi_A}{M}\frac{\tau b_1 RT}{\varepsilon D_{AB}} + \frac{3}{4}\frac{\tau b_1}{d\varepsilon}\sqrt{\frac{2\pi RT}{M}})^{-1} \quad (12)$$

Here M represents molecular mass of water vapour; χ_A is defined as mole fraction of the vapour; ε represents membrane porosity; D_{AB} is defined as the diffusivity of water vapour (A) in the air (B); b_1 represents the membrane thickness; τ represents the average membrane tortuosity; d represents the mean diameter for the hollow fibre membrane pore; R represents the universal gas constant; and T is the mean temperature within the hollow fibre membrane pores.

D_{AB} can be determined from [23, 24]:

$$D_{AB} = \frac{1.895*10^{-5}T^{2.072}}{P} \quad (13)$$

Here, P is defined as the total pressure.

χ_A can be determined by [21]:

$$\chi_A = \frac{P_v}{P} \quad (14)$$

Here P_v represents the partial pressure for the water vapour.

The tortuosity (τ) is estimated by [25] :

$$\tau = \frac{(2\text{-}\varepsilon)^2}{\varepsilon} \tag{15}$$

With the combination of Eqs. (10) and (12), the flux $J_{vm,i}$ can be written as:

$$J_{vm,i} = \left(\frac{1-\chi_A}{M}\frac{\tau b_1 RT}{\varepsilon D_{AB}} + \frac{3}{4}\frac{\tau b_1}{d\varepsilon}\sqrt{\frac{2\pi RT}{M}}\right)^{-1}(P_{fm,i} - P_{pm,i}) \tag{16}$$

Therefore, N_i can also be expressed by:

$$N_i = 7.58*10^{-5}\frac{d\varepsilon}{\tau b_1}\frac{MT^{1.072}}{4Rd(P-Pv)+5.685*10^{-5}T^{1.072}\sqrt{2\pi MRT}} \tag{17}$$

The heat transfer of the slice *i* through the hollow fibre membrane can be divided into sensible heat transfer via heat conduction and latent heat transfer, which is described by:

$$Q_3 = [\frac{\lambda_2}{b_1}(T_{fm,i} - T_{pm,i}) + J_{vm,i}h_{latent}]L_2 N_f N_g dx_i \tag{18}$$

Combining Eqs. (11) and (18) gives:

$$Q_3 = [\frac{2\pi\lambda_2}{\ln(r_3/r_1)}(T_{fm,i} - T_{pm,i}) + J_{vm,i}h_{latent}\frac{2\pi(r_3 - r_1)}{\ln(r_3/r_1)}]N_f N_g dx_i \tag{19}$$

Here Q_3 represents the total heat transfer through hollow fibre of slice *i*; h_{latent} represents the latent heat of vaporization for water; λ_2 represents average thermal conductivity for hollow fibre, which is determined by:

$$\lambda_2 = (1-\varepsilon)\lambda_m + \varepsilon\lambda_{air} \tag{20}$$

Here λ_m and λ_{air} represent the membrane material thermal conductivity and air thermal conductivity, respectively.

2.1.3 Mass and heat transfers within the permeate gap

The water vapour is distilled into permeate at the interface of permeate and membrane, the mass transfer of slice *i* can be described by:

$$\Delta\dot{m}_{fb,i} = \dot{m}_{pg,i} - \dot{m}_{pg,i+1} = J_{pg,i}L_3 N_f N_g dx_i \tag{21}$$

Here $J_{pg,i}$ is defined as the water vapour flux for slice i in permeate gap; and $\dot{m}_{pg,i+1}$ and $\dot{m}_{pg,i}$ represent the permeate mass flow rates coming in and out of slice i, respectively, because the permeate flows in opposite direction to the hot feed flow.

To analyse the heat transfer phenomenon in the gap channel, Gao et al. [9] found that the permeate within the gap channel was nearly stagnant, therefore, the convective heat can be neglected, and the heat transfer was mainly caused by conduction, which can be determined by:

$$Q_4 = \frac{2\pi\lambda_3}{\ln(r_5 / r_3)}(T_{pm,i} - T_{pc,i})N_f N_g dx_i \qquad (22)$$

Here Q_4 represents the heat transfer rate within the permeate gap of slice i; λ_3 represents the permeate thermal conductivity; $T_{pc,i}$ is the interface temperature between the cooling plate and permeate of slice i ; and r_5 represents the inner radius of the cooling plate.

2.1.4 Heat transfer through the cooling plate

The heat is transferred through the cooling plate to the coolant side, this process can be described by:

$$Q_5 = \frac{2\pi\lambda_4}{\ln(r_7 / r_5)}(T_{pc,i} - T_{cc,i})N_g dx_i \qquad (23)$$

Here, Q_5 represents total heat transfer through the cooling plate of slice i; λ_4 represents the cooling plate thermal conductivity; $T_{cc,i}$ is the interface temperature between the coolant and cooling plate of slice i ; and r_7 represents the outer radius of the cooling plate.

2.1.5 Heat transfer within the coolant channel

The heat transfer from the cooling plate surface to the coolant bulk flow of slice i can be expressed by:

$$Q_6 = \alpha_{c,i}(T_{cc,i} - T_{cb,i})L_7 N_g dx_i \qquad (24)$$

Here, Q_6 represents the total heat transfer from the cooling plate surface to the coolant bulk flow of slice i; $T_{cb,i}$ is the temperature for the bulk coolant flow of slice i; and $\alpha_{c,i}$ represents the heat transfer coefficient on the coolant side, it can be obtained similarly as $\alpha_{f,i}$; and L_7 is the circumference of the cooling plate based on its outer radius (r_7). Here, because the heat transfer from cooling plate to coolant occurs at the interface between coolant and cooling plate, and the coolant flows through the cooling plate shell side, cooling plate outer radius r_7 is used to calculate the interface surface area for heat transfer in coolant channel.

The heat transfer of slice i for the coolant bulk flow can be calculated as:

$$Q_7 = \dot{m}_{cb,i} C_{pcb,i} T_{cb,i} - \dot{m}_{cb,i+1} C_{pcb,i+1} T_{cb,i+1} \tag{25}$$

Here, Q_7 represents total heat transfer for the coolant bulk flow of slice i; $\dot{m}_{cb,i}$ and $\dot{m}_{cb,i+1}$ are the bulk coolant mass flow rates coming out and into the slice i, respectively; $C_{pcb,i}$ and $C_{pcb,i+1}$ are defined as the specific heat capacities of coolant bulk flow coming out and into the slice i, respectively; and $T_{cb,i}$ and $T_{cb,i+1}$ are temperatures for coolant bulk flow coming out and into the slice i, respectively.

2.2 Numerical solutions

The following assumptions have been made to simulate the heat and mass transfers of hollow fibre PGMD module:

- no heat loss to the surrounding atmosphere via the module shell;
- no heat loss due to the permeate production from the system;
- no changes in membrane porosity, thickness, and tortuosity;
- the heat transfer phenomenon within gap channels is mainly caused by conduction; and
- gap width is constant for the gap between hollow fibre and cooling plate.

Due to the complicated geometry of the air gap in hollow fibre AGMD module, various hollow fibre AGMD modelling studies [26, 27] made the assumptions that hollow fibres are uniformly distributed and they have the same distance to the cooling plate. This is only an ideal approximation as hollow fibres are usually distributed randomly with different distances to the cooling plate across the air gap [28, 29]. The above assumptions are also applied in our hollow fibre PGMD study during the mathematical modelling.

Based on the above assumptions, it can be concluded that:

$$Q_1 = Q_2 = Q_3 = Q_4 = Q_5 = Q_6 = Q_7 = Q_{trans} \tag{26}$$

Here, Q_{trans} represents the total heat transfer of slice i.

From Eqs. (4), (18), (22), (23) and (24), the following equations can be obtained:

$$\frac{Q_2}{\alpha_{f,i} L_1 N_f N_g dx_i} = T_{fb,i} - T_{fm,i} \tag{27}$$

$$\frac{\dfrac{Q_3}{L_2 N_f N_g dx_i} - J_{vm,i} h_{latent}}{\dfrac{\lambda_2}{b_1}} = T_{fm,i} - T_{pm,i} \tag{28}$$

$$\frac{Q_4}{\dfrac{2\pi\lambda_3}{\ln(r_5 / r_3)} N_f N_g dx_i} = T_{pm,i} - T_{pc,i} \tag{29}$$

$$\frac{Q_5}{\dfrac{2\pi\lambda_4}{\ln(r_7 / r_5)} N_g dx_i} = T_{pc,i} - T_{cc,i} \tag{30}$$

$$\frac{Q_6}{\alpha_{c,i} L_7 N_g dx_i} = T_{cc,i} - T_{cb,i} \tag{31}$$

Combining Eqs. (27 – 31) gives:

$$Q_{trans} = U(T_{fb,i} - T_{cb,i} + J_{vm,i} h_{latent} \frac{b_1}{\lambda_2}) \tag{32}$$

Here, U can be determined by:

$$U = \left(\frac{1}{\alpha_{f,i} L_1 N_f N_g dx_i} + \frac{1}{L_2 N_f N_g dx_i}\frac{b_1}{\lambda_2} + \frac{1}{\frac{2\pi\lambda_3}{\ln(r_5/r_3)} N_f N_g dx_i} + \frac{1}{\frac{2\pi\lambda_4}{\ln(r_7/r_5)} N_g dx_i} + \frac{1}{\alpha_{c,i} L_7 N_g dx_i}\right)^{-1} \quad (33)$$

Considering a vertical module, the hot feed is assumed to flow into the module from the top, and the coolant flows counter-currently from the bottom. Thus, the input conditions, the inlet temperatures for the coolant and feed, are at different x-positions. In order to solve the differential equations for the mass and heat transfers, a matching scheme from the feed inlet X=0 requires a value for the coolant exit temperature, which is an unknown to begin with. To start the numerical solution, an initial guess of $T_{cb,1}$ is made, which is generally the average temperature of the hot and coolant inlet temperatures. Based on this assumption, the solution can be marched till the exit of the feed at Xn=l and an estimated coolant inlet temperature can be obtained. When the difference between the estimated and actual coolant inlet temperatures is more than 0.00001 ˚C, the solution process is repeated with a new guess on the coolant exit temperature at X=0 until convergence. A flowchart of the numerical solution process is shown in Fig.3.

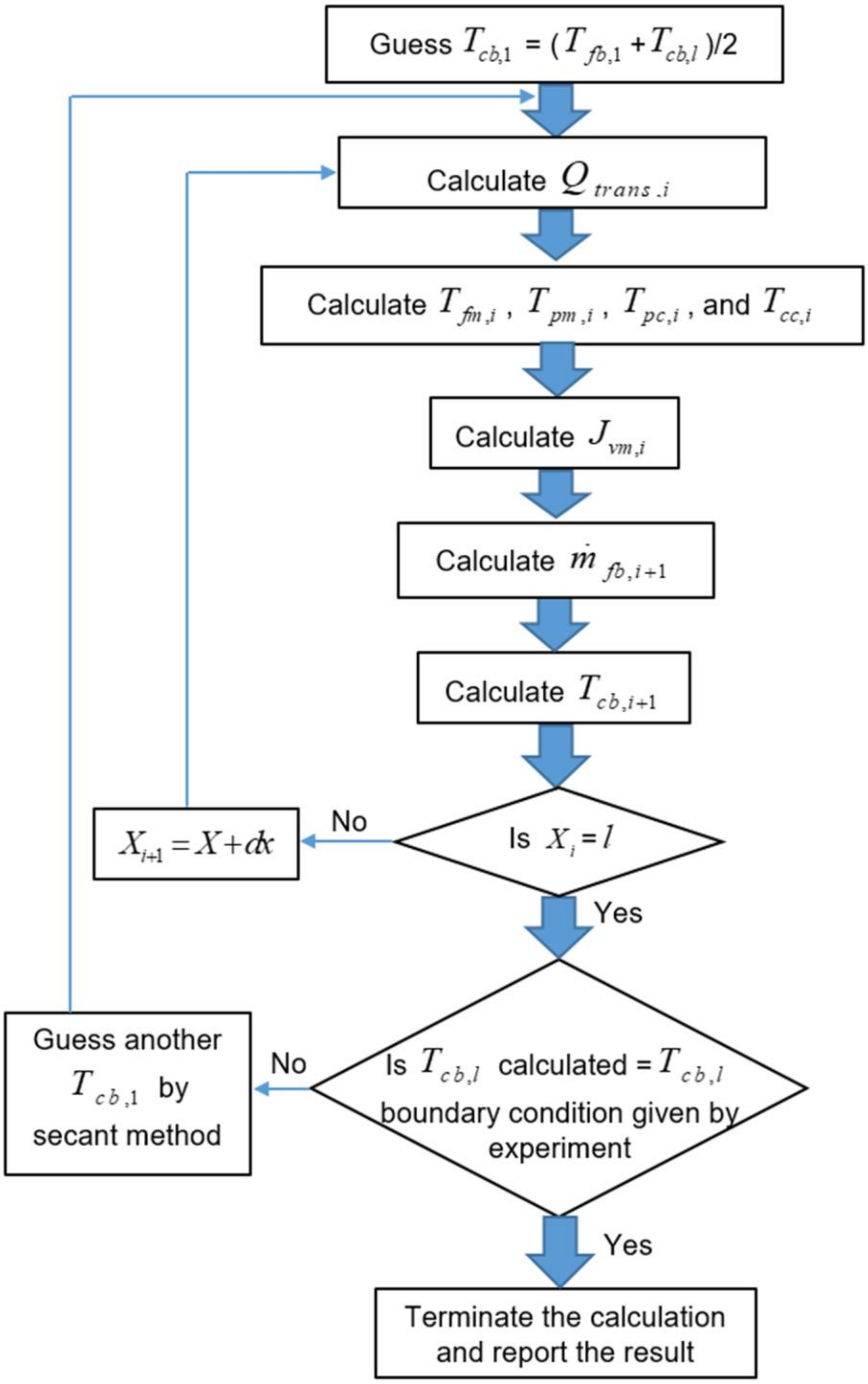

Fig. 3. Simulation procedure for hollow fibre PGMD model

3. Material and experiments

3.1 Employed membrane and modules

Hollow fibre membrane were purchased from Tianjin Polytechnic University. The fibres were previously examined [9] and a summary of its properties can be found in Table 1. The inner surface contact angle and outer surface contact angle were 132º and 94º, respectively, which demonstrate the hydrophobic property of the employed membrane. The relatively high

Liquid Entry Pressure (LEP) and membrane porosity also make the employed membrane suitable for MD application.

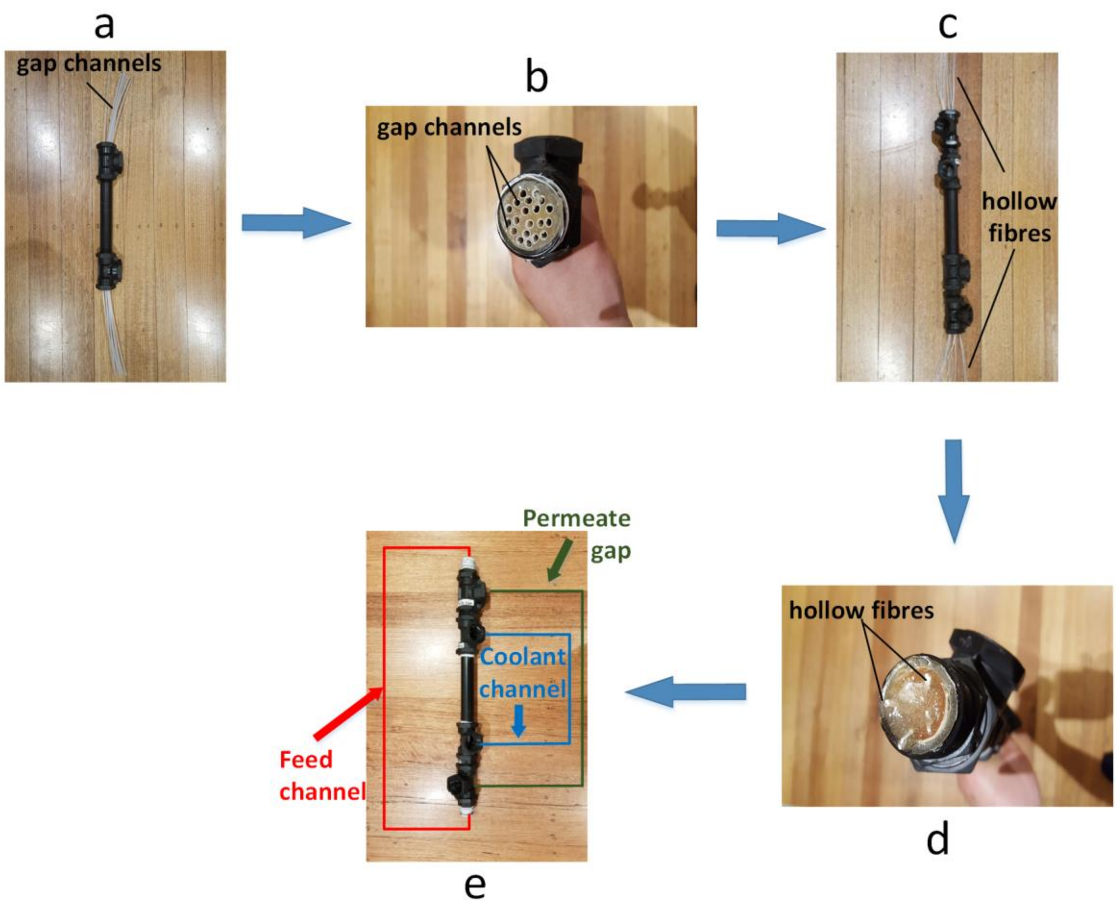

Fig. 4. Fabrication of hollow fibre PGMD module

Fig. 4 shows the detailed structure of hollow fibre PGMD module. As the fabrication process of PGMD module has been described previously [20], a brief summary is provided here. Firstly, High Density Polyethylene (HDPE) or Stainless Steel (SS) tubes were inserted into the module shell (PE pipe) to establish the permeate gap channels (Fig. 4a). After fixing by the epoxy resin compound, the excess HDPE or SS pipes were trimmed off (Fig. 4b). Different numbers of hollow fibres were then inserted into each gap channel and potted by epoxy resin compound subsequently (Fig. 4c). The excess hollow fibre were also trimmed off to finalize the module fabrication (Figs. 4d and 4e).

It is worthwhile mentioning that great efforts have been made to 1) set the hollow fibre in the center of the gap channel (1 hollow fibre), (b) uniformly distribute the hollow fibres within the gap channel (2-3 hollow fibres), and (c) keep the hollow fibre as straight as possible to prevent the hollow fibres from sticking to each other or to the inner surface of the gap channel. However, as the lab-scale testing modules, it is difficult to perfectly control the gap width (gap between hollow fibre and gap channel), especially when the hollow fibre packing density becomes higher.

Tables 2 and 3 show the detailed properties of different modules and gap channels, respectively. Table 4 shows the experimental operating conditions.

3.2 PGMD testing

Experiments with various operating conditions were undertaken to validate the developed mathematical model. The process flow diagram for PGMD experiments is shown in Fig. 5.

Because the PGMD experiments have been explained in [9] and [20], only a brief description is provided here. Due to the separation between the coolant and the produced permeate, brine was used for both the hot feed and coolant. The brine was pumped through coolant channel (membrane shell side) firstly and hot channel (membrane lumen side) subsequently using a single peristaltic pump, which could save pump energy consumption compared to other conventional MD processes. The gap channels were flooded by the permeate, the excessive permeate flowed into a distillate reservoir. Based on the change of the distillate reservoir weight over time (2-4 hours after flux stabilization), the flux can be estimated. Other testing conditions can be found in Table 4.

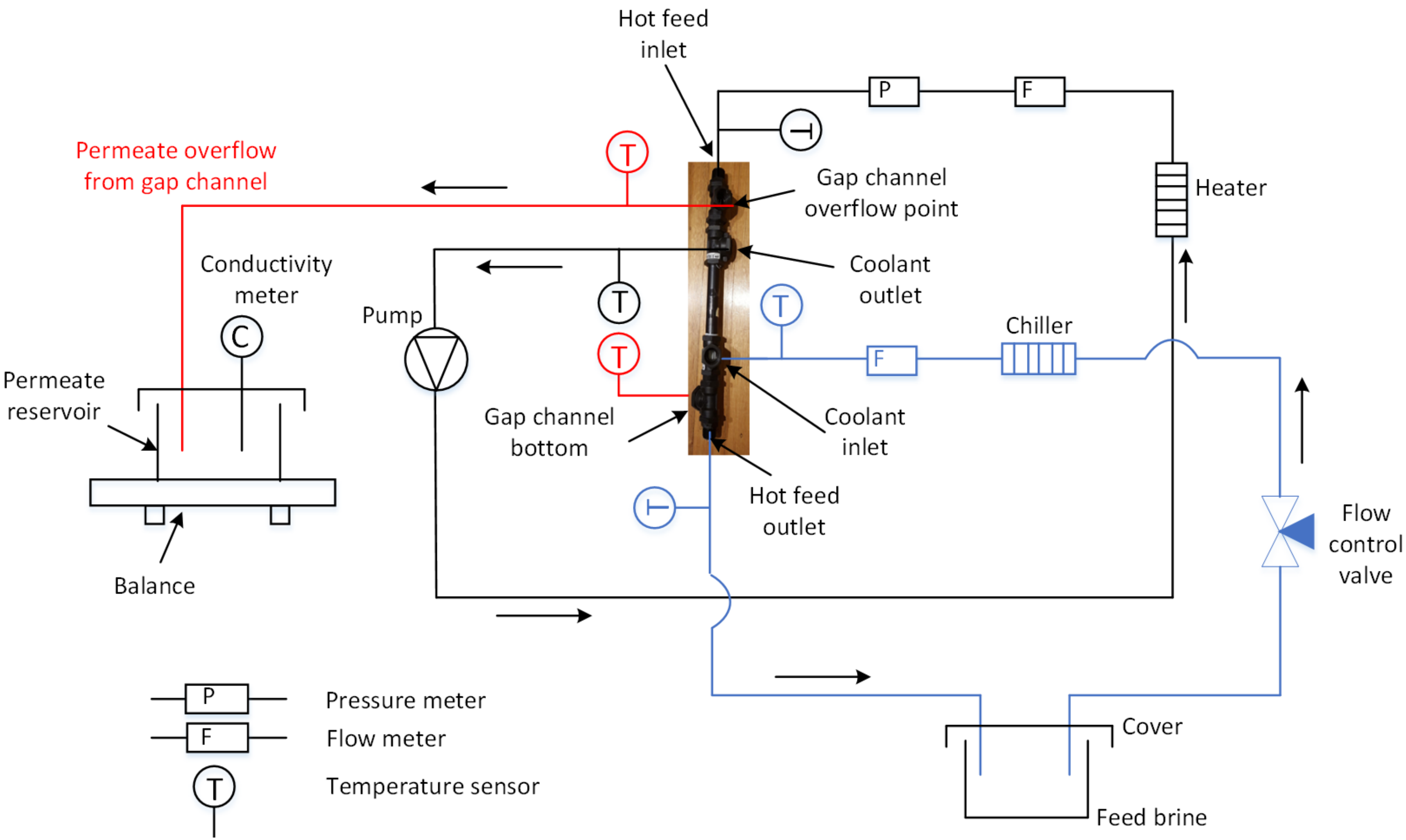

Fig. 5. Process flow diagram for PGMD experiments

Table 1 Characteristics of employed hollow fibre membrane

Material	Manufacture method	Dimension (mm)			Mean pore size (μm)	Porosity (%)	LEP (kPa)	Contact angle ($^\circ$)	
		Inner diameter	Outer diameter	Thickness				Inner	Outer
Polyvinylidene Fluoride (PVDF)	Non-solvent Induced Phase Separation (NIPS) process	0.81	1.11	0.15	0.15	81.7	240.8	132 $\pm$ 3	94 $\pm$ 2

Table 2 Properties of manufactured hollow fibre membrane modules

Module number	Material of cooling plate	Number of gap channels	Percentage of PE pipe occupied by gap channels (%)	Number of hollow fibres within each channel	Percentage of single gap channel occupied by hollow fibre membrane (%)	Length of module (m)	Surface area of hollow fibre membrane (m^2)
1	HDPE	8	14.8	1	15.3	0.35	0.0084
2	HDPE	8	14.8	2	30.6	0.35	0.0167
3	HDPE	8	14.8	3	45.8	0.35	0.0251
4	SS	8	51.6	1	6.0	0.35	0.0084

Table 3 Properties of gap channels

	Inner diameter (mm)	Outer diameter (mm)	Thickness b_2 (mm)	Conductivity λ_4 (W/m.K)
HDPE gap channel	2.84	3.40	0.28	0.445 [20]
SS gap channel	4.55	6.35	0.90	15 [20]

Table 4 PGMD testing conditions

	Inlet temperature (˚C)	Volumetric flow rate (mL/min)	Brine concentration (g/L NaCl)
Hot channel	40, 50, 60, 70	70-500 (0.28-0.69 m/s)	10
Coolant channel	20	70-500 (0.003-0.020 m/s)	10

4. Result and discussion

4.1 Model validation with experimental data

To check the accuracy of the developed model, the experimental data is compared with the predicted results from the model.

Experimental results of module 1 (8 HDPE gap channels, and each gap channel holds 1 hollow fibre inside) are used to validate the effects of feed inlet temperature and velocity.

Fig. 6 shows that the experimental data of module 1 obtained with different velocities but a fixed hot inlet temperature (70 ˚C) are very close to the simulated results obtained from the model, and Table 5 demonstrates that the errors between the experimental outcomes and modelled results are in the range of approximately ±5%, which are smaller than the typical experimental error of ±10%. The model predicts an asymptotic flux trend as the feed velocity increases. This phenomenon has been identified by many other studies [14, 30, 31], which is mainly due to temperature polarization being unable to be further reduced for a fully-developed flow condition. Furthermore, the concentration polarization is higher with the increasing flux [32], which will adversely affect the vapour pressure.

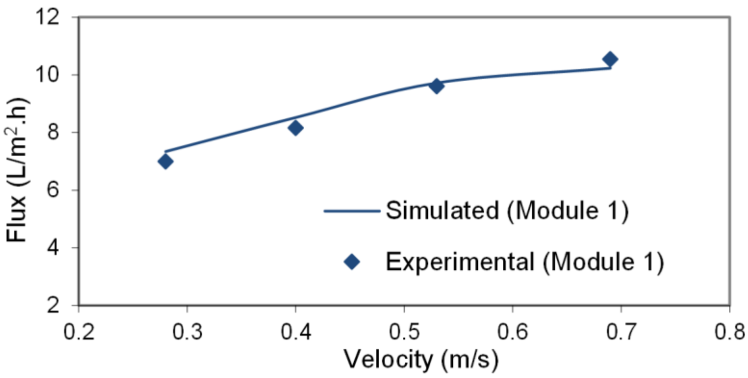

Fig. 6. Simulated and measured results with different feed velocities (70 ˚C hot inlet temperature)

Table 5 Relative errors between predicted and experimental results (70 ˚C hot inlet temperature)

Hot feed velocity (m/s)	0.28	0.40	0.53	0.69
Error (%)	-5.04	-4.46	-1.18	2.89

Fig. 7 demonstrates that the difference between modelled results and experimental results of module 1 obtained with a fixed feed velocity (0.69 m/s) but different hot inlet temperatures. The comparison (Table 6) shows that, again, the model predictions agree with the experimental results to within ±10% for the given experimental conditions. The model also successfully predicts a more significant flux increase with higher feed inlet temperature, which is attributed to the fact that vapour pressure increases exponentially with feed inlet temperature [33, 34].

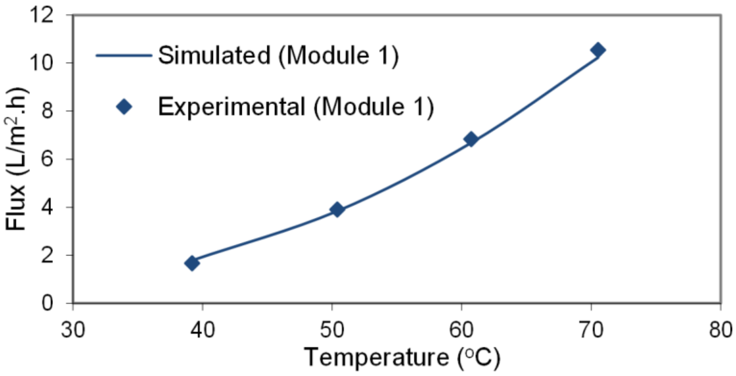

Fig. 7. Simulated and measured results with different feed inlet temperatures (0.69 m/s feed velocity)

Table 6 Relative errors between predicted and experimental results (0.69 m/s feed velocity)

Feed inlet temperature (˚C)	**40**	**50**	**60**	**70**
Error (%)	-6.93	1.58	2.25	2.89

Both Tables 5 and 6 show that the relative errors systematically increase from less than zero to larger than zero as the flux increases when feed velocity and feed temperature become greater. This phenomenon is probably attributed to the assumption of ‘no heat loss due to the permeate production’. Increased flux in the experiments will result in more heat loss in the permeate gap and lower the temperature in the gap channel. As a result, the actual temperature within the permeate gap will be lower than the modelled temperature. Since the flux is predicted based on the temperatures in the feed and permeate gaps, the lower predicted temperature difference would lead to a lower flux than that of the experiments.

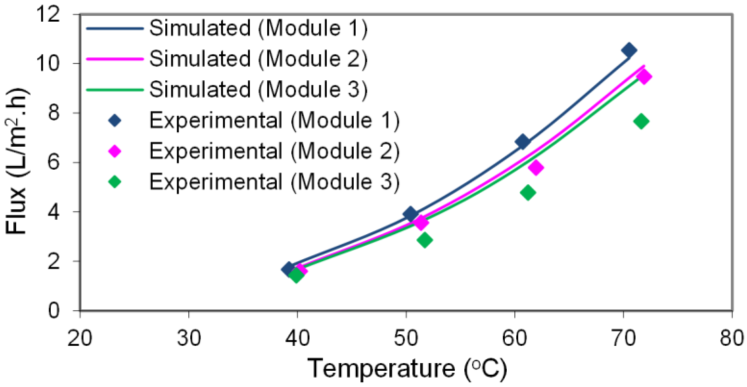

Fig. 8. Simulated and measured results with different hollow fibre densities (0.69 m/s feed velocity)

Table 7 Relative errors between predicted and experimental results (0.69 m/s feed velocity)

Feed inlet temperature (˚C)		**40**	**50**	**60**	**70**
	Module 1	-6.93	1.58	2.25	2.89
Error (%)	Module 2	-9.22	-4.84	-10.46	-4.61
	Module 3	-15.87	-28.93	-26.55	-23.55

Experimental and simulated results of modules 1, 2 and 3 at various hot inlet temperatures can be found in Fig. 8. Similar to module 1, both module 2 and module 3 have 8 gap channels. A single gap channel of module 2 and 3 are filled by 2 and 3 hollow fibres, respectively. The simulated flux decreases as a function of fibre packing density, which is confirmed by the experimental results. This phenomenon can be explained by two main reasons [20]. Firstly, more permeate will be produced for the module with larger membrane surface area (higher hollow fibre density), which results in greater temperature increase in the gap channel and reduced vapour pressure difference across the hydrophobic membrane. In addition, a higher fibre packing density could lead to a less effective membrane surface area for permeate production as the hollow fibres could be attached to each other. Furthermore, a lower hollow fibre density will cause less dead mixing zone within the module due to the existence of transverse flow [35].

Table 7 shows that the differences between simulated and experimental results for modules 1 and 2 are within approximately ±10%, while the differences for module 3 are much larger (-20% to -30%). This phenomenon could be mainly attributed to the modelling assumptions that hollow fibres are uniformly distributed and they have the same distance to the cooling plate across the water gap. The outer diameter of hollow fibre membrane and the inner diameter of HDPE gap channel are 1.11 mm and 2.84 mm, respectively. When 3 hollow fibres are inserted into the gap channel, the hollow fibres will inevitably be in contact with each other or to the inner surface of the cooling plate, the hollow fibres lose their full contact with fluids and the dead mixing zones are created. Compared to the experimental results, the model predicts the flux under optimal conditions, and subsequently, overestimates the flux. The error of the prediction becomes greater when hollow fibre density is higher as contact between fibres becomes more likely. In order to reduce the effects of these assumptions, baffles or spacers could be used within the PGMD module to help the uniform distribution of the hollow fibres.

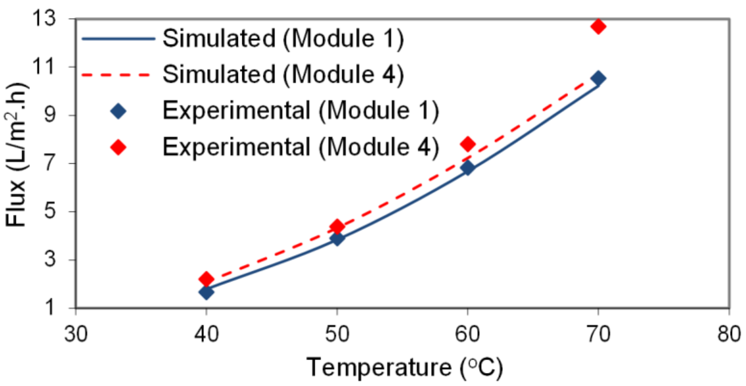

Fig. 9. Simulated and measured results with different cooling plate materials (0.69 m/s feed velocity)

Table 8 Relative errors between predicted and experimental results (0.69 m/s feed velocity)

Feed inlet temperature (˚C)		**40**	**50**	**60**	**70**
Error (%)	Module 1	-6.93	1.58	2.25	2.89
	Module 4	5.49	1.25	7.42	15.24

The simulated and experimental results of modules 1 and 4 with different cooling plate materials are presented in Fig. 9. The model predicts that a higher flux can be achieved for the module made of SS cooling plate. Similar results are obtained from experiments. Previous study [20] advises that the sensible heat transfer is proportional to the ratio of cooling plate thermal conductivity (λ_4) to the thickness of cooling plate (b_2), the value of $\frac{\lambda_4}{b_2}$ for HDPE cooling plate is significantly lower compared to that of SS cooling plate, indicating a lower thermal resistance for module 4. This will subsequently lead to a bigger vapour pressure difference between the hydrophobic membrane surfaces and higher flux for module 4. Table 8 shows that the difference between simulated and experimental results are all within ±10%, except for one result of module 4 at 70 ˚C hot inlet temperature (15%). Aforementioned, this high error was probably attributed to the higher heat loss because of the increased flux (higher permeate production).

In addition to the thermal conductivity and thickness, the SS gap channel has different inner and outer diameters compared to HDPE gap channel, which will change the hydrodynamics within the coolant channel and permeate gap simultaneously. To understand the effects of different design parameters (inner/outer diameters and conductivity of gap channel) on flux, a sensitivity study based on the developed model was undertaken, which is further discussed in Section 4.2.4.

4.2 Effects of design parameters and operating conditions

The validation and discussion shown in Section 4.1 demonstrate that the developed model can successfully simulate the mass and heat transfers within hollow fibre PGMD module. The model is now utilized to analyze the effects of other important module design parameters and operating conditions on flux and energy efficiency. The outcome will help to optimize hollow fibre PGMD process.

The effects of feed inlet temperature and feed velocity on flux and energy efficiency of PGMD have been extensively discussed in our previous investigation [9], this simulation study focuses on the effects of coolant inlet temperature, coolant velocity and cooling plate materials on flux and energy efficiency of PGMD module.

Here, the energy efficiency of PGMD module is indicated by Specific Thermal Energy Consumption (STEC), which is the thermal energy required to produce 1 kg of permeate water. It can be calculated by:

$$STEC = \frac{\dot{Q}_{heat}}{\dot{m}_{pg}} \quad (34)$$

Here, $\dot{Q}_{heat}$ is defined as the external thermal power input, and it can be calculated by the coolant outlet temperature and hot inlet temperature.

To facilitate the discussion, the simulated results obtained from a base case (case 1) is compared to the results based on other designs or operating conditions. Module 1 operated with 0.69 m/s hot feed velocity and 70 ˚C feed inlet temperature is used as the base case (case 1).

4.2.1 Effect of coolant velocity

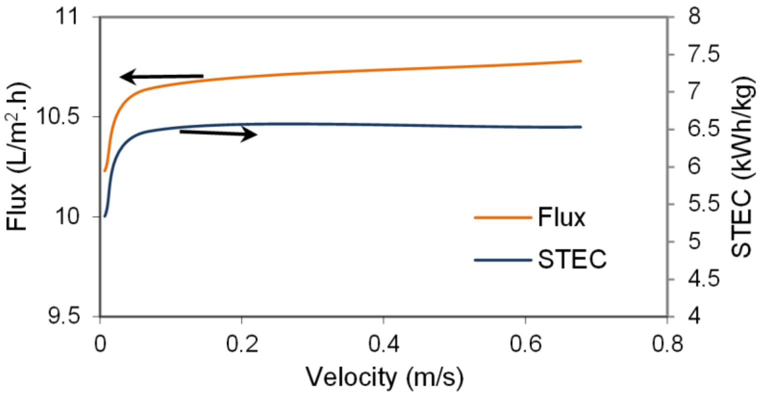

Fig. 10. Effect of coolant velocity on flux and STEC (0.69 m/s hot feed velocity and 70 ˚C hot inlet temperature)

Due to the unique module characteristics, PGMD module normally has the same flowrate for coolant and feed flows, and the effect of coolant flow rate has not been extensively investigated compared to DCMD module.

Our hollow fibre PGMD module was tested under a one-pump system, the volumetric flowrate of coolant is the same as that of the hot feed. The cross sectional area of feed channels is considerably smaller than that of cold channel, therefore, the coolant velocity is approximately one to two orders of magnitude lower than hot feed velocity (see Table 4) [20]. Temperature polarization of the coolant channel is high due to the extremely low coolant velocity (velocity: 0.003 – 0.007 m/s, Re: 30 – 74). To understand the impact of coolant velocity on PGMD performance, the model was used to simulate flux and STEC with higher coolant velocity.

Fig. 10 shows that flux only increases 4.0% and 5.4% when the coolant velocity increases 10 (0.068 m/s) and 100 times (0.68 m/s) compared to that of case 1 (0. 0068 m/s), showing a minimum impact of coolant velocity. Here, the hot feed velocity remains constant at 0.69 m/s during all simulations. Other studies [30, 36] evaluated the effect of cold permeate velocity on flux for DCMD systems. They concluded that cold permeate velocity has insignificant impact on flux compared to feed velocity since the feed side is the source of vapourization and controls the permeation process [36]. For PGMD module, the coolant does not contact with membrane directly and its effect on flux is expected to be lower. Furthermore, coolant velocity has no impact on the temperature polarization in the gap channels, consequently, the effect of coolant velocity on permeate is minimum.

It can also be seen from Fig. 10 that the STEC increases approximately by 21.2% when the coolant velocity increases from 0.0068 m/s to 0.068 m/s, and further increase in coolant velocity will result in a minimum increase in STEC. Lu et al. [32] studied the effect of distillate velocity on specific energy consumption using DCMD module, which included both thermal energy consumption and pumping energy consumption. Similar to our results, they identified that the specific energy consumption for heating increased with increasing distillate flow rate. In our study, a higher coolant velocity will lead to a lower coolant outlet temperature, and therefore, more external thermal energy is required to heat the brine to the pre-set hot feed inlet temperature. Although the flux is higher with the increasing coolant velocity, the increase in thermal energy input is more rapid than the increase of flux, consequently, STEC increases as a function of coolant velocity. When the coolant velocity is higher than 0.068 m/s, the coolant outlet temperature is very close to the coolant inlet temperature (20 ˚C), further increase in coolant velocity will not result in a significant change in external thermal energy input, as a result, a minimum increase in STEC is observed with the further increase in coolant velocity.

4.2.2 Effect of coolant inlet temperature

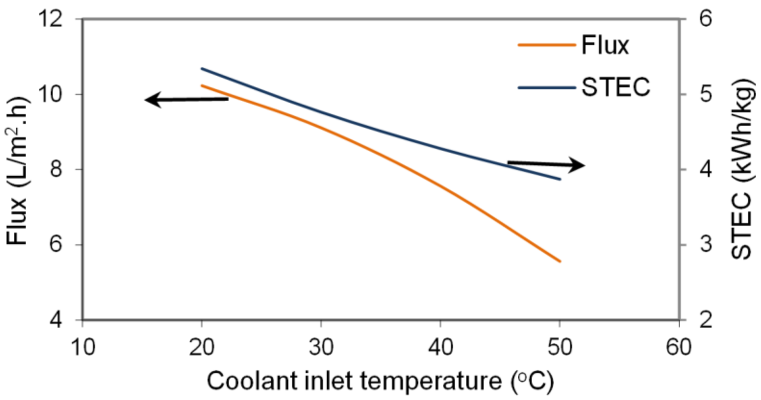

Fig. 11. Effect of coolant inlet temperature on flux and STEC (0.69 m/s hot feed velocity and 70 ˚C hot inlet temperature)

Fig. 11 shows the effects of coolant inlet temperature on flux and STEC. It can be seen clearly that the flux decreases as a function of coolant inlet temperature, and it decreases more significantly at higher coolant inlet temperature. This is due to the exponential relationship between vapour pressure difference and temperature difference across the membrane. Furthermore, compared to the effect of hot inlet temperature on flux shown in Fig. 7, the coolant inlet temperature has a less impact on flux. Cheng et al. [18] used hollow fibre membrane module to compare the performance of AGMD with PGMD. They identified the similar results as the flux increased exponentially with increasing hot inlet temperature but only decreased gradually with increasing coolant inlet temperature.

Alklaibi et al. [30] reviewed the impacts of coolant inlet temperature of various MD studies. They suggested that changes in coolant temperature can result in more than a 1-fold increase in flux (inlet temperature difference between hot and coolant channels: 30 – 50 ˚C), although the effect of coolant inlet temperature was considerably lower compared to that of hot inlet temperature. In our study, there is less than a 1-fold improvement of flux when the coolant inlet temperature changes from 50 ˚C to 20 ˚C. This indicates that coolant inlet temperature for hollow fibre PGMD has even less effect on flux compared to DCMD. This phenomenon is due to the permeate gap of PGMD module adding to the heat transfer resistance, so a temperature decrease in the cold channel cannot effectively change the vapour pressure difference between the membrane surfaces. Furthermore, this phenomenon makes PGMD module more suitable for multi-stage application. The coolant effluent from an upstream stage can be used as the coolant influent for the next stage in multi-stage processes, and the flux does not decrease significantly when coolant temperature increases along the stages.

It can also be seen from Fig. 11 that the STEC decreases as a function of coolant inlet temperature, from 5.34 kWh/kg at 20 ˚C coolant inlet temperature to 3.87 kWh/kg at 50 ˚C coolant inlet temperature. With a higher coolant inlet temperature, a lower external energy input is required, and the external thermal energy input decreases more rapidly than the decrease of flux, as a result, STEC decreases with the increasing coolant inlet temperature.

4.2.3 Effect of cooling plate thermal conductivity

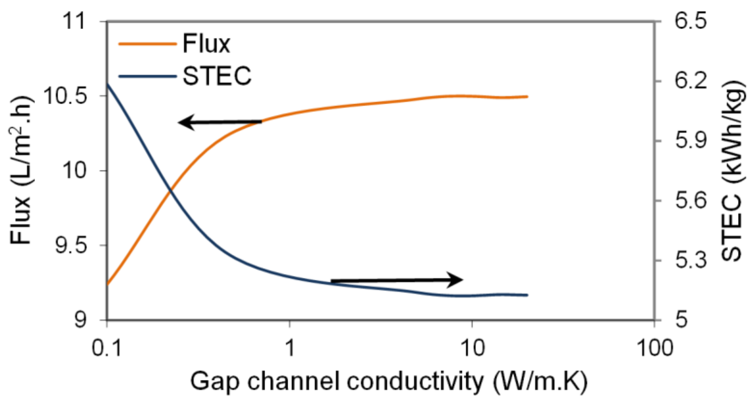

Fig. 12. Effect of cooling plate thermal conductivity on flux and STEC (0.69 m/s hot feed velocity and 70 ˚C hot inlet temperature)

Fig. 12 demonstrates the effect of cooling plate thermal conductivity on flux and STEC. The coolant inlet temperature of 20 ˚C, hot inlet temperature of 70 ˚C, and hot feed velocity of 0.69 m/s were used as the inputs for the model. The cooling plate thermal conductivity was changed from 0.1 W/m.K to 20 W/m.K.

Fig. 12 shows that the flux and STEC are 14% higher and 17% lower, respectively, when the thermal conductivity of cooling plate changes from 0.1 W/m.K to 5 W/m.K, and there is no significant changes in flux and STEC when cooling plate thermal conductivity increases beyond 5 W/m.K. With a higher cooling plate thermal conductivity, the heat transfer from the gap channel to coolant channel is enhanced, the temperature in the gap channel becomes lower, but the temperature within the coolant channel is higher. Thus, the flux will be higher due to the greater temperature difference between membrane surfaces, but less external thermal energy input is required because of the better internal thermal energy recovery.

Fig. 13 shows the temperature profiles for modules 1 and 4 with 0.69 m/s hot feed velocity and 70 ˚C hot inlet temperature. It clearly shows that the temperature difference across the cooling plate for module 1 (between T_{cc} and T_{pc}) is approximately 4 ˚C, but the temperature difference across the cooling plate for module 4 is less than 0.2 ˚C. This indicates that if the cooling plate thermal conductivity is high enough, the interface temperature between the coolant and cooling plate (T_{cc}) is nearly the same as the interface temperature between the permeate and the cooling plate (T_{pc}). Further increase in cooling plate thermal conductivity will not significantly improve the heat transfer through the cooling plate and permeate gap, and subsequently, the flux and STEC will not be improved significantly.

a) HDPE cooling plate thermal conductivity of 0.445 W/m.K

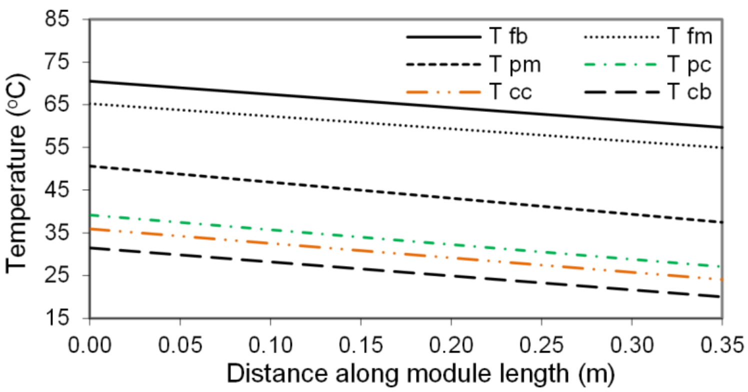

b) SS cooling plate thermal conductivity of 15 W/m.K

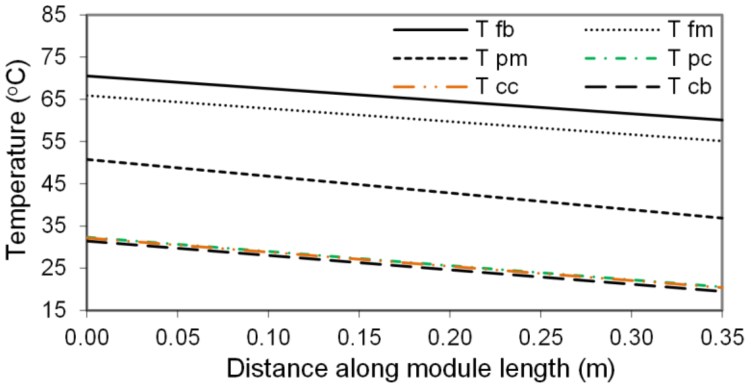

Fig. 13. Temperature profiles for modules 1 and 4 (0.69 m/s hot feed velocity and 70 ˚C hot inlet temperature)

Fig. 14 shows further details on the effect of cooling plate thermal conductivity on temperature difference between the cooling plate surfaces. It is suggested that 5 W/m.K is considered as the critical thermal conductivity value for the cooling plate. When the cooling plate thermal conductivity is higher than 5 W/m.K, the heat transfer resistance through cooling plate becomes negligible, and therefore, it has minimum impact on flux and STEC.

In addition to the high conductivity cooling plate, other highly conductive materials (such as metal mesh) could be inserted into permeate gaps to further improve hollow fibre PGMD performance.

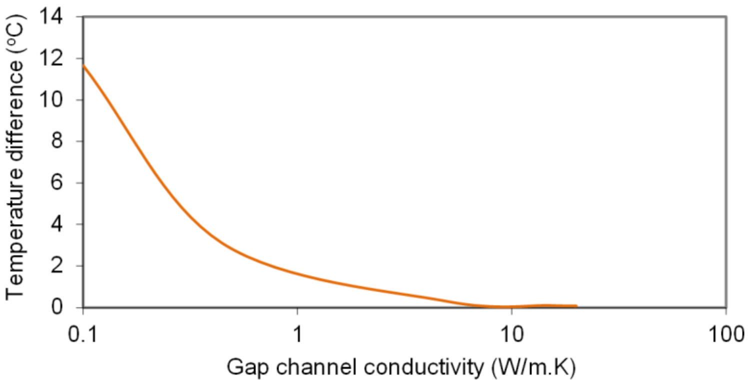

Fig. 14. Effect of cooling plate thermal conductivity on temperature difference across cooling plate (0.69 m/s hot feed velocity and 70 ˚C hot inlet temperature)

4.2.4 Sensitivity study of different gap channel properties

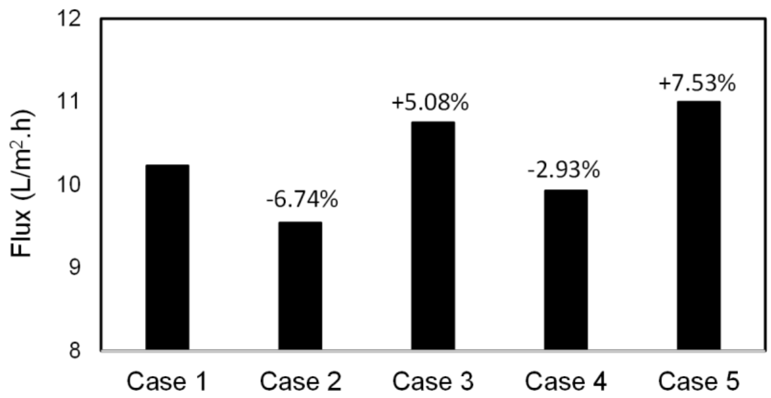

Fig. 15. Sensitivity study of different design parameters (inner/outer diameters and conductivity of gap channel)

During the PGMD experiments, it was identified that module 1 made of HDPE cooling plate had a lower flux compared to that of module 4 made of SS cooling plate. It was suggested this is mainly caused by the higher thermal conductivity of SS compared to HDPE. The simulated results also show the similar outcomes.

The HDPE gap channel had a smaller inner/outer diameters compared to the SS gap channel, consequently, the hydrodynamics of coolant and permeate gaps will be influenced in addition to the thermal conductivity when SS gap channel is used to replace HDPE gap channel. Here, a typical One-At-A-Time approach was used to evaluate the effects of different parameters (gap channel conductivity, gap channel inner dimeter and outer dimeter) on PGMD performance.

Table 9 shows the model inputs for design variables of 5 cases. As mentioned before, the base case (case 1) is based on module 1 with HDPE gap channel operated with 0.69 m/s hot feed velocity and 70 ˚C hot inlet temperature.

Table 9 Design parameters of sensitivity analysis

	Gap channel conductivity (W/m.K)	Gap channel inner diameter (mm)	Gap channel outer diameter (mm)
Case 1	0.445	2.84	3.40
Case 2	0.445	2.84	6.35
Case 3	15	2.84	6.35
Case 4	0.445	1.60	3.40
Case 5	15	1.60	3.40

Fig. 15 shows the flux of each case and the percentage of relative flux change based on case 1.

For case 2, the gap channel conductivity and gap channel inner diameter are kept the same as case 1, but the gap channel outer dimeter is increased to 6.35 mm, which is the same as SS gap channel outer diameter. The simulated results show that the flux of case 2 is 6.74% lower than that of case 1. The larger outer dimeter of gap channel will result in a better hydrodynamic flow within the coolant channel due to the higher coolant velocity, but it will also lead to a higher thermal resistance of the gap due to the larger thickness. Because of the lower flux of case 2, it can be concluded that the higher thermal resistance plays a more important role compared to the better hydrodynamics. This phenomenon could be attributed to two possible reasons. Firstly, although the coolant velocity of case 2 (0.019 m/s) is approximately 1.8 times higher than that of case 1 (0.0068 m/s), the decrease of temperature polarization for case 2 is limited as the coolant is still under laminar flow. Secondly, the gap thermal conductivity is low and a thicker gap will result in a higher thermal resistance.

Compared to case 2, the gap channel thermal conductivity is increased to 15 W/m.K from 0.445 W/m.K, the inner and outer diameters of the gap are still 2.84 mm and 6.35 mm for case 3, respectively. The simulated result from Fig. 15 shows that the flux for case 3 is 5.08% higher than that of case 1. This result confirms that the gap channel thermal conductivity has a more critical role compared to cold velocity.

For case 4, the gap thermal conductivity and gap channel outer dimeter are the same as those of case 1, but the gap channel inner dimeter is decreased to 1.60 mm. The model result shows a minor decrease of flux (2.93%) compared to case 1. This phenomenon can be explained by the fact that HDPE gap channel has a slightly lower thermal conductivity (0.445 W/m.K) compared to that of water (0.6 W/m.K at 20 ˚C). The flow within the permeate gap is nearly stagnant [9], as a result, the permeate within the gap channel can be considered as an annular layer outside of the hollow fibre membrane. For case 4, when the gap channel inner dimeter is decreased, the thickness of the water annular layer is decreased and the thickness of gap channel with lower thermal conductivity is increased. Consequently, the overall thermal resistance of gap channel and water layer is higher, and flux is decreased accordingly.

For case 5, the gap channel inner and outer diameters are the same as those of case 4, but the thermal conductivity of gap channel increases to 15 W/m.K. The simulated result shows a 7.53% increase in flux of case 5 compared to case 1. Similarly, this phenomenon is due to the overall less thermal resistance of the gap channel and water layer.

Both Francis et al. [7] and Khalifa [14] investigated the effect of gap width on PGMD performance using flat sheet membrane modules. Francis et al. [7] identified that the effect of gap width on flux was negligible. On the contrary, Khalifa [14] found that a higher gap width generally reduced the flux because of the increased heat transfer resistance. Compared to the above flat sheet PGMD studies, the changes in gap channel (inner/outer diameters and thermal conductivity) of hollow fibre PGMD module in our study result in a more complex combination (hydrodynamics in coolant and permeate gaps and thickness of gap channel). Based on the above discussion, it is suggested that the larger outer diameter of the gap channel can benefit the hydrodynamic flow within coolant channel, but its effect on flux is very low when the gap channel thermal conductivity is low. The effect of gap channel inner diameter on permeate gap hydrodynamic flow is negligible, because the permeate overflow velocity is extremely low. Overall, the gap thermal resistance plays a more important role in PGMD performance.

4.2.5 Effect of multi-stage process on energy efficiency

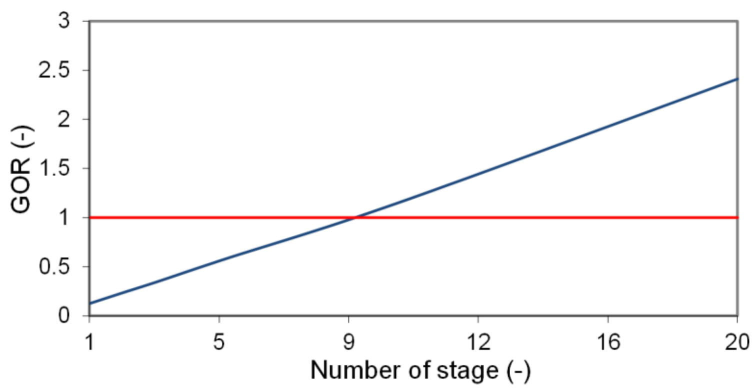

Fig. 16. Effect of number of stages on energy efficiency

Compared to a single stage process, a multi-stage process will maximize the internal heat recovery of PGMD to improve energy efficiency. Furthermore, it is still possible to utilize the high velocity to improve the flux and decrease the temperature polarization [20].

Here, the effect of multi-stage process on energy efficiency of module 1 is evaluated using the developed model. In the simulation, multiple PGMD modules (module 1) are connected in series. The brine is cooled to a pre-set temperature before flowing through the cold channel of the first module. It is then pumped through each module's cold channel and comes out from the last membrane module. Afterwards, the brine enters into the hot channel of the last module via a heater. It flows reversely to the first module through the hot channel of each module. The following values are used as the model inputs: the coolant and feed velocities are 0.0068 m/s and 0.69 m/s, respectively; the coolant and hot inlet temperatures are 20 ˚C and 70 ˚C, respectively (here, the flowrates of feed and coolant are identical).

Gain Output Ratio (GOR) is used here to indicate the energy efficiency of PGMD module. When GOR is higher than 1, it demonstrates the process can save thermal energy rather than the pure evaporation process with no heat recovery [37].

GOR can be calculated by:

$$GOR = \frac{\dot{m}_{pg} \cdot h_{latent}}{\dot{Q}_{heat}} \quad (35)$$

Fig. 16 shows that the GOR increases as the number of stages increases, from 0.12 with a 1 stage unit to 2.4 with a 20 stage unit. When there are more than 9 stages of PGMD modules, the GOR becomes higher than 1. Cipollina et al. [17] used a predictive model to simulate the behavior of multi-stage flat sheet PGMD and found that GOR can increase 20 times from a 1 stage unit to a 9 stage unit, and may reach a value between 3 and 4. With a similar flowrate (200 mL/min), GOR from their study became more than 1 with a 3 stage unit, which is much less than that of our study. They suggested that the most energy efficient system should have more stages with larger membrane surface area. The effective membrane surface area of the single module from their study is 0.042 m^2, which is 5 times larger than that of our hollow fibre PGMD module. Consequently, the GOR of their module reaches 1 with only 3 stages. Module 1 from this study has relatively low densities for hollow fibres and permeate gaps, but a full scale hollow fibre membrane module normally has a higher hollow fibre density and larger specific surface area [20], which will result in an increased GOR value.

4.3 Roles of different parameters in PGMD optimization

An optimal PGMD module design should result in a higher flux and better energy efficiency, however, various studies [38-40] observed a trade-off between flux and energy efficiency, because it is difficult to obtain a better energy efficiency and high flux simultaneously. The discussion in Section 4.2 confirms that change in one parameter (or operating condition) could lead to the beneficial effect on flux and unfavourable result in energy efficiency, but the degree of influence could be different. To evaluate the roles of different parameters in PGMD optimization, an indicator 'flux equivalent (flux.eqv)' is used here to combine the flux and GOR into one parameter.

Introduced by Liu et al. [41], flux.eqv can be calculated by:

$$flux.eqv = flux * GOR \quad (36)$$

Mathematical simulation is undertaken with different inputs for various design parameters, the flux.eqv is then calculated, and the ideal condition is determined for the design with the highest flux.eqv. As mentioned in Section 4.2, this study only focuses on the effects of coolant velocity, coolant inlet temperature and cooling plate thermal conductivity on flux and energy efficiency, and 0.69 m/s feed velocity and 70 ˚C hot inlet temperature are used as the inputs for optimization study. The gap channel density and hollow fibre packing density are the same as those of module 1. Other model inputs for different design variables could be found from Table 10.

Based on the simulation results, the deviation from the optimal condition (percentage of relative flux.eqv change) can be determined and the roles of different parameters in PGMD optimization can be evaluated.

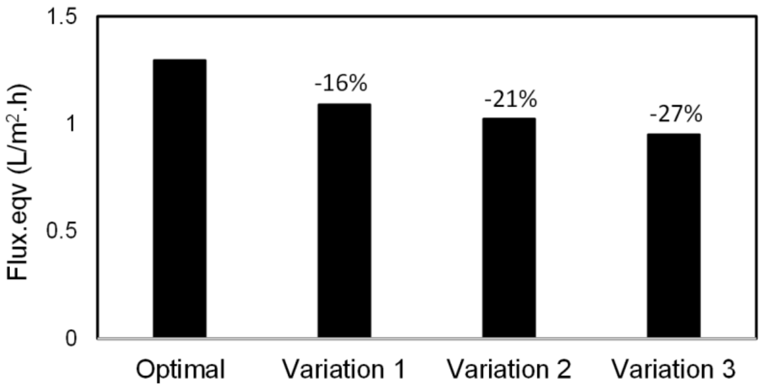

Fig. 17. Roles of different parameters in PGMD optimization

For the variation 1, the coolant velocity is 100 times higher than that of the optimal condition, other model inputs are the same as optimal condition. With the higher coolant velocity, flux will be higher, but the increase in flux is not adequate to compensate the decrease in GOR, as a result, flux.eqv is 16% lower. For the variation 2, with the higher coolant inlet temperature, the energy efficiency (GOR) is higher, similarly, the increase in GOR is not enough to compensate the decrease of flux, because flux decreases exponentially with decreasing temperature difference across the membrane. For variation 3, with a lower cooling plate thermal conductivity, both flux and GOR will be lower, the flux.eqv is 27% lower than that of the optimal condition.

Table 10 Model inputs of different design variables for optimization study

	Coolant inlet temperature (˚C)	Coolant velocity (m/s)	Cooling plate thermal conductivity (W/m.K)
Optimal	20	0.0068	5
Variation 1	20	0.68	5
Variation 2	50	0.0068	5
Variation 3	20	0.0068	0.1

Based on the above discussion, it could be suggested that the cooling plate thermal conductivity plays the most important role in PGMD optimization. The increase of cooling plate thermal conductivity has beneficial effects on both flux and energy efficiency. Compared to the coolant velocity, coolant inlet temperature has a more significant impact on PGMD performance, which is probably due to two main reasons. Firstly, flux has an exponential relationship with the temperature difference across the membrane, although the effect of coolant inlet temperature in PGMD is expected to be lower than that of DCMD. Secondly, coolant is not in direct contact with the membrane, the temperature / concentration polarizations cannot be effectively decreased by the increasing coolant velocity.

5. Conclusions

In this study, the mass and heat transfers of hollow fibre PGMD module was simulated using a mathematical model. The model has been firstly validated by experimental results, and the difference between simulated results and experimental results were within the experimental error range except for the high hollow fibre packing density when the model overestimates the flux. The main reason for this phenomenon is that the model simulates the flux under optimal situation where hollow fibre has the full contact with both feed and permeate, but actually the fibres may touch each other leading to a reduced effective membrane area.

The validated model was then utilized to evaluate the effects of various design parameters and operating conditions on PGMD performance. It is identified that coolant velocity and coolant temperature have less impact on flux compared to those of DCMD, because the coolant of DCMD contacts with membrane directly. Furthermore, the coolant velocity of PGMD is extremely low, so it is difficult to decrease the temperature polarization of coolant channel effectively.

The model also suggests that the higher flux and better energy efficiency could be obtained for the module with highly conductive cooling plate. However, when the cooling plate thermal conductivity is higher than 5 W/m.K, the temperature difference across the cooling plate is minimum and further increases in the cooling plate thermal conductivity has the negligible impacts on flux and STEC. In application, the use of highly conductive material needs to be balanced with the cost.

A sensitivity study is undertaken to analyze the combined effects of gap channel inner/outer diameters and gap channel thermal conductivity on flux. It is concluded that the changes in gap channel (inner/outer diameters and thermal conductivity) of hollow fibre PGMD module will result in a more complex combination (hydrodynamics in coolant and permeate channels and thickness of gap channel) compared to other flat sheet PGMD studies, and the gap thermal conductivity has a more significant effect on flux compared to the hydrodynamic flows within the permeate and coolant channels.

The effect of multi-stage processes on energy efficiency is evaluated by the developed model. The results suggest that the GOR increases as increasing number of stages, it reaches 2.4 for a 20 stage unit. The energy performance could be further improved when higher gap channel density or hollow fibre density is applied.

The roles of different parameters in PGMD optimization is finally discussed, taking both flux and energy efficiency into consideration. Based on the modelling results, it could be suggested that cooling plate thermal conductivity plays the most important role in PGMD optimization compared to the coolant velocity and coolant inlet temperature.

Funding

Funding support from South East Water and Coliban Water's R&D programs is gratefully acknowledged.

Acknowledgements

We sincerely thank Dr. Dharma Dharmabalan for his advice on the experimental setup.

[1] G. Amy, N. Ghaffour, Z. Li, L. Francis, R.V. Linares, T. Missimer, S. Lattemann, Membrane-based seawater desalination: Present and future prospects, Desalination, 401 (2017) 16-21.
[2] R. Schwantes, A. Cipollina, F. Gross, J. Koschikowski, D. Pfeifle, M. Rolletschek, V. Subiela, Membrane distillation: Solar and waste heat driven demonstration plants for desalination, Desalination, 323 (2013) 93-106.
[3] N. Dow, S. Gray, J.-d. Li, J. Zhang, E. Ostarcevic, A. Liubinas, P. Atherton, G. Roeszler, A. Gibbs, M. Duke, Pilot trial of membrane distillation driven by low grade waste heat: Membrane fouling and energy assessment, Desalination, 391 (2016) 30-42.
[4] N. Thomas, M.O. Mavukkandy, S. Loutatidou, H.A. Arafat, Membrane distillation research & implementation: Lessons from the past five decades, Separation and Purification Technology, 189 (2017) 108-127.
[5] P. Wang, T.-S. Chung, Recent advances in membrane distillation processes: Membrane development, configuration design and application exploring, Journal of Membrane Science, 474 (2015) 39-56.
[6] G. Yang, Z. Xie, M. Cran, D. Ng, S. Gray, Enhanced desalination performance of poly (vinyl alcohol)/carbon nanotube composite pervaporation membranes via interfacial engineering, Journal of Membrane Science, 579 (2019) 40-51.
[7] L. Francis, N. Ghaffour, A.A. Alsaadi, G.L. Amy, Material gap membrane distillation: A new design for water vapor flux enhancement, Journal of Membrane Science, 448 (2013) 240-247.
[8] J. Swaminathan, H.W. Chung, D.M. Warsinger, F.A. AlMarzooqi, H.A. Arafat, J.H. Lienhard V, Energy efficiency of permeate gap and novel conductive gap membrane distillation, Journal of Membrane Science, 502 (2016) 171-178.
[9] L. Gao, J. Zhang, S. Gray, J.-D. Li, Experimental study of hollow fiber permeate gap membrane distillation and its performance comparison with DCMD and SGMD, Separation and Purification Technology, 188 (2017) 11-23.
[10] D. Winter, J. Koschikowski, S. Ripperger, Desalination using membrane distillation: Flux enhancement by feed water deaeration on spiral-wound modules, Journal of Membrane Science, 423-424 (2012) 215-224.
[11] D. Winter, J. Koschikowski, M. Wieghaus, Desalination using membrane distillation: Experimental studies on full scale spiral wound modules, Journal of Membrane Science, 375 (2011) 104-112.
[12] M. Essalhi, M. Khayet, Application of a porous composite hydrophobic/hydrophilic membrane in desalination by air gap and liquid gap membrane distillation: A comparative study, Separation and Purification Technology, 133 (2014) 176-186.
[13] V.V. Ugrozov, I.B. Elkina, V.N. Nikulin, L.I. Kataeva, Theoretical and experimental research of liquid-gap membrane distillation process in membrane module, Desalination, 157 (2003) 325-331.
[14] A.E. Khalifa, Water and air gap membrane distillation for water desalination – An experimental comparative study, Separation and Purification Technology, 141 (2015) 276-284.
[15] F. Mahmoudi, H. Siddiqui, M. Pishbin, G. Goodarzi, S. Dehghani, A. Date, A. Akbarzadeh, Sustainable Seawater Desalination by Permeate Gap Membrane Distillation Technology, Energy Procedia, 110 (2017) 346-351.
[16] A. Ruiz-Aguirre, J.A. Andrés-Mañas, J.M. Fernández-Sevilla, G. Zaragoza, Modeling and optimization of a commercial permeate gap spiral wound membrane distillation module for seawater desalination, Desalination, 419 (2017) 160-168.
[17] A. Cipollina, M.G. Di Sparti, A. Tamburini, G. Micale, Development of a Membrane Distillation module for solar energy seawater desalination, Chemical Engineering Research and Design, 90 (2012) 2101-2121.
[18] L. Cheng, Y. Zhao, P. Li, W. Li, F. Wang, Comparative study of air gap and permeate gap membrane distillation using internal heat recovery hollow fiber membrane module, Desalination, 426 (2018) 42-49.

[19] F. Mahmoudi, G.M. Goodarzi, S. Dehghani, A. Akbarzadeh, Experimental and theoretical study of a lab scale permeate gap membrane distillation setup for desalination, Desalination, 419 (2017) 197-210.
[20] L. Gao, J. Zhang, S. Gray, J.-D. Li, Influence of PGMD module design on the water productivity and energy efficiency in desalination, Desalination, 452 (2019) 29-39.
[21] A.S. Alsaadi, N. Ghaffour, J.D. Li, S. Gray, L. Francis, H. Maab, G.L. Amy, Modeling of air-gap membrane distillation process: A theoretical and experimental study, Journal of Membrane Science, 445 (2013) 53-65.
[22] H. Chang, C.-D. Ho, J.-A. Hsu, Analysis of Heat Transfer Coefficients in Direct Contact Membrane Distillation Modules Using CFD Simulation, Journal of Applied Science and Engineering, 19 (2016) 197-206.
[23] J. Phattaranawik, Effect of pore size distribution and air flux on mass transport in direct contact membrane distillation, Journal of Membrane Science, 215 (2003) 75-85.
[24] J. Zhang, S. Gray, J.-D. Li, Modelling heat and mass transfers in DCMD using compressible membranes, Journal of Membrane Science, 387-388 (2012) 7-16.
[25] A. Alkhudhiri, N. Darwish, N. Hilal, Membrane distillation: A comprehensive review, Desalination, 287 (2012) 2-18.
[26] C. Guijt, G. Meindersma, T. Reith, A. Dehaan, Air gap membrane distillation1. Modelling and mass transport properties for hollow fibre membranes, Separation and Purification Technology, 43 (2005) 233-244.
[27] R. Aryapratama, H. Koo, S. Jeong, S. Lee, Performance evaluation of hollow fiber air gap membrane distillation module with multiple cooling channels, Desalination, 385 (2016) 58-68.
[28] L.-Z. Zhang, Conjugate Heat and Mass Transfer in Heat Mass Exchanger Ducts, 1 ed., Academic Press, Waltham, USA, 2014.
[29] L.-Z. Zhang, Heat and mass transfer in a randomly packed hollow fiber membrane module: A fractal model approach, International Journal of Heat and Mass Transfer, 54 (2011) 2921-2931.
[30] A.M. Alklaibi, N. Lior, Membrane-distillation desalination: Status and potential, Desalination, 171 (2005) 111-131.
[31] J. Zhang, J.-D. Li, M. Duke, Z. Xie, S. Gray, Performance of asymmetric hollow fibre membranes in membrane distillation under various configurations and vacuum enhancement, Journal of Membrane Science, 362 (2010) 517-528.
[32] K.J. Lu, Z.L. Cheng, J. Chang, L. Luo, T.-S. Chung, Design of zero liquid discharge desalination (ZLDD) systems consisting of freeze desalination, membrane distillation, and crystallization powered by green energies, Desalination, 458 (2019) 66-75.
[33] J. Xu, Y.B. Singh, G.L. Amy, N. Ghaffour, Effect of operating parameters and membrane characteristics on air gap membrane distillation performance for the treatment of highly saline water, Journal of Membrane Science, 512 (2016) 73-82.
[34] P. Wang, M.M. Teoh, T.-S. Chung, Morphological architecture of dual-layer hollow fiber for membrane distillation with higher desalination performance, Water Research, 45 (2011) 5489-5500.
[35] X. Yang, R. Wang, L. Shi, A.G. Fane, M. Debowski, Performance improvement of PVDF hollow fiber-based membrane distillation process, Journal of Membrane Science, 369 (2011) 437-447.
[36] A. Khalifa, H. Ahmad, M. Antar, T. Laoui, M. Khayet, Experimental and theoretical investigations on water desalination using direct contact membrane distillation, Desalination, 404 (2017) 22-34.
[37] D. Winter, J. Koschikowski, F. Gross, D. Maucher, D. Düver, M. Jositz, T. Mann, A. Hagedorn, Comparative analysis of full-scale membrane distillation contactors - methods and modules, Journal of Membrane Science, 524 (2017) 758-771.
[38] J. Swaminathan, H.W. Chung, D.M. Warsinger, J.H. Lienhard V, Membrane distillation model based on heat exchanger theory and configuration comparison, Applied Energy, 184 (2016) 491-505.
[39] M. Gryta, M. Tomaszewska, The capillary MD module integrated with a heat exchanger, Inzynieria Chemiczna I Procesowa, 20 (1999) 221-233.

[40] D. Cheng, N. Li, J. Zhang, Modeling and multi-objective optimization of vacuum membrane distillation for enhancement of water productivity and thermal efficiency in desalination, Chemical Engineering Research and Design, 132 (2018) 697-713.
[41] Z. Liu, Q. Gao, X. Lu, L. Zhao, S. Wu, Z. Ma, H. Zhang, Study on the performance of double-pipe air gap membrane distillation module, Desalination, 396 (2016) 48-56.